Hindawi
International Journal of Aerospace Engineering
Volume 2020, Article ID 3906375, 14 pages
https://doi.org/10.1155/2020/3906375

Research Article

Analysis of the Influence of Trace Point Step-Jump Behavior

Yao Yang,[1] Yang Xu ,[2] and Pei Wang[1]

[1]*Aerospace Institute, Northwestern Polytechnical University, Xi'an, Shaanxi, China*
[2]*Hypervelocity Aerodynamics Institute, China Aerodynamics Research and Development Center, Mianyang, Sichuan, China*

Correspondence should be addressed to Yang Xu; mingze0108@126.com

Received 15 January 2020; Revised 17 August 2020; Accepted 5 September 2020; Published 19 October 2020

Academic Editor: Giulio Avanzini

To explore the influence of the trace point step-jump behavior on a terminal guidance system, an analysis is performed from the line-of-sight rate (LOS rate) and guidance accuracy views for designing an anti-step-jump guidance law. First, the linear terminal guidance model under the trace point jump circumstance is constructed, and then the fundamental reason for the miss distance is investigated by deriving the upper bound of the LOS rate at the initial step-jump moment. Following this, the novel proposed analytical differential adjoint model is established with the adjoint method, and its validity is demonstrated comparing with the numeric derivative model. Based on the adjoint model, the effects of the ratio coefficient, the time constant, and the jump amplitude on the guidance accuracy are explored. Finally, a novel anti-step-jump guidance law is designed to shorten the recovery time of the overload. The simulations have shown that the faster recovery time and higher accuracy are achieved in comparison with the proportional navigation guidance, optimal guidance, and adaptive sliding mode guidance.

1. Introduction

Accurately discriminating and localizing the interest points, steadily tracking the target, and processing with good timeliness are the main properties of optical detecting systems [1–3]. Infrared (IR) seeker, as an important member, has received great attention due to its increasing use in air combat [4, 5]. Statistics suggest that infrared-seeking missiles have been responsible for more than 80% of the combat aircraft losses over the past 40 years [6]. To confront the IR system, different IR countermeasures are subsequently produced and applied to the battlefield [7–9]. However, we know that there are a lot of factors that can mitigate the striking capabilities and increase the likelihood of successful evasion, aside from IR flares, such as various target maneuvers, possible disturbances, and measurement noise [10–12]. They all perform as a kind of persistent excitation and result in a continuous disturbance to the missile system. To cope with these problems, a considerable amount of studies has been carried out to find approximate optimal solutions, such as, for the maneuvering concern, Lin and Chen [13] and Li and Qian [14] successively designed high-precision guidance laws to intercept high-speed and maneuvering targets by introducing an adaptive fuzzy algorithm, respectively. With the same purpose, Lee et al. [15] proposed a dual mode guidance using the proportional navigation (PN) guidance and the swarm optimization algorithm. A positive result with obvious advantages to the PN guidance was achieved according to the change rate of the LOS rate. Meanwhile, for the disturbance problem, Du et al. [12] analyzed the influence of different disturbance rejection rate models to the infrared seeker and confirmed the significance of the disturbance to the guidance system. Next, a terminal guidance law based on the stochastic fast smooth second-order sliding mode method is proposed by considering the stochastic disturbance [16]. Besides, for the various possible measurement noise issue, Xu et al. [17] proposed an efficient Gaussian mixture filter based on the prune-cluster-merge scheme to deal with the glint noise. Additionally, other types of filters have also been put forward, like robust Student's t mixture probability hypothesis density filter processing the heavy-tailed noises [18] and so on [19, 20]. To this end, the strategies to the continuous disturbance have been effectively designed, and it is naturally of interest to reduce the effects of IR flares.

IR flares are considered as the most effective countermeasure method by generating the false radiation signals and

deflecting the missile by the gradually separated combustion [21, 22]. Actually, the effects of flares mainly include two aspects: one is disturbing the seeker system to prevent the missile from recognizing true targets and the other is disturbing the guidance system by generating abnormal overload signals and causing the missile to become unstable. To tackle the first matter, Li et al. [23] utilized the Bayesian method to build a probabilistic recognition model, which is more efficient than the feature template matching approach. Likewise, Wu et al. [24] revealed the inherent structure and infrared signature of the aircraft and provided an anti-interference method after exploiting the occlusion detection. The final results showed that the proposed aircraft-tracking method performed favourably against state-of-the-art trackers. After that, White [25] emphasized that the movement feature could be a feasible recognition reference for the flare belonging to an off-board countermeasure, and Wang et al. [26] proposed an intelligent algorithm, which considered the combined invariant moments as the image features, succeeding in recognizing the target under the certain error conditions by using a BP neural network. As yet, the research on the recognition algorithm is still on the way and achieves lots of promising results. At the same time, to lower the effects of flares on the guidance system, researchers started from the countermeasure mechanism, and in this process, the recognition problems are neglected. Firstly, based on the assumption of small LOS angle, Zarchan [27] creatively introduced the adjoint model to derive the relationship between the miss distance and the parameters of the guidance system. It is worth remarking that Zarchan is the first one to treat the IR countermeasure problem as a multiple target problem, and more importantly, it gives a detailed description about the engagement. Following this, the effects of maneuvers and noise to the miss distance were analyzed [28], and then an analytical expression between the miss distance and some influencing factors was derived when the target takes maneuvers and throws flares simultaneously [29]. Meanwhile, Gutman [30] proved the stability of the adjoint system, which further promoted the adjoint theory to the practical applications. However, as the imperative parameter of the guidance system, little attention has been devoted to abnormal change of the LOS rate variable.

Cognizant of this problem, this paper analyzes the effects of flares from the LOS rate caused by the step-jump behavior and designed a novel anti-step-jump guidance law, the main contributions of which can be summarized as follows. First, the adjoint method is introduced to construct the step-jump behavior of the trace point. Second, the reason for the step-jump behavior is revealed and its influence on the LOS rate and miss distance is analyzed with the proposed analytic derivative adjoint model, respectively. Afterwards, an influence analysis on the influencing factors is conducted on the terminal guidance system under the step-jump circumstance. Finally, a novel anti-step-jump guidance law is proposed to alleviate the countermeasure effects and promote the guidance precision.

The remainder of this paper proceeds as follows. In Section 2, the confrontation model is presented and the step-jump behavior is introduced. The effect of flares on the LOS rate is analyzed in Section 3. In Section 4, we provide the numeric derivative model and analytic adjoint model to give analysis of the influencing factors. Section 5 discusses the performance of the anti-step-jump guidance. Conclusions and future work are given in Section 6.

2. Problem Description

First, we will provide a brief background on the engagement. For an imaging seeker, it tends to average the signal when the radiation sources overlaps with each other, and the optical axis directs towards the central of gravity of the IR radiation intensity within each exposure. Once the overlap effects no longer work, the target may be recognized by specific features with a high probability. The overlap effects are depicted as follows.

In Figure 1, the yellow point is the energy centroid that the seeker tracks, the red and green shapes represent the IR flares, and the gray shape denotes the target of interest. As shown in Figure 1(a), the target and the flare are separated far from each other, which is readily available to position the target by a specific recognition algorithm. While in Figure 1(b), the two objects are overlapped with each other. According to [21, 31], these two objects are detected as one, which makes the seeker not able to recognize the true target. Then, the seeker will resolve the position of the energy centroid and track it. As the energy of the flare is much stronger than the target, so the energy centroid is much closer to the flare. Figure 1(c) depicts a dual-overlap effect wherein the follow-up flare overlaps the target and the preceding flare simultaneously, which makes the former flare continue to work. Hence, the tracking point directs to the energy centroid of three objects.

Meanwhile, for the recognition algorithm, the features of energy, average gray feature, length-width ratio, and compactness are commonly employed to identify the target [31], and their definitions are given in Table 1.

In Table 1, $E_{i,j}$ represents the energy of the pixel (i, j), parameter s denotes the number of pixels in the target image area, and parameters l and w are the length and width of the circumscribed rectangle around the target image area, respectively. It should be noted that the first two features reflect the energy characteristic, and the others represent the geometric characteristic. Virtually, more characteristics are beneficial to improve the recognition probability of the target, but due to the computation constraints and the timeliness requirement, here, we only select four features as a reference. The tracking process is then shown in Figure 2.

Figure 2 describes a typical side-tailed attack situation by dispensing a single flare each time. The red cross is the tracking point, and the yellow pane is the monitor window for capturing the interested radiation source. The monitor window enlarges when the flare overlaps the target, such as the 516-th frame and 793-th frame, or the angle between the flare and the aircraft is smaller than the angle resolution of the seeker, as seen in the 253-th frame. Additionally, the cross points to the position that is close to the flare when the seeker is not able to recognize the target. In this process, the corresponding LOS rate and overload are shown in Figure 3.

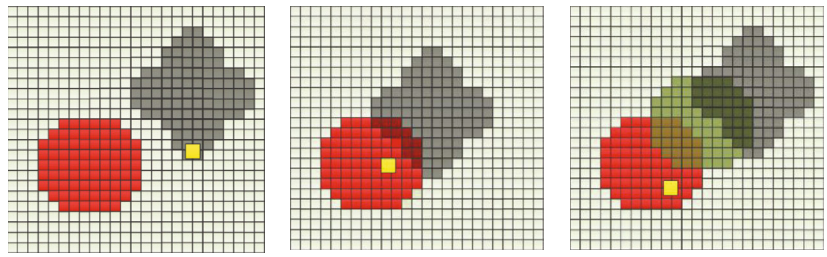

(a) (b) (c)

Figure 1: Relationships between objects in different positions: (a) nonoverlapping condition; (b) two overlapping objects detected as one; (c) three overlapping objects detected as one.

Table 1: Definition of the image feature.

Feature	Meaning	Definition
c_1	Energy	$c_1 = \sum_{j=1}^{m}\sum_{i=1}^{n} E_{i,j}$
c_2	Average gray	$c_2 = \frac{c_1}{s}$
c_3	Length-width ratio	$c_3 = \frac{l}{w}$
c_4	Compactness	$c_4 = \frac{s}{l \cdot w}$

As shown in Figure 3(a), the LOS rate is slightly decoyed by the flare countermeasure. As the target is distinguished, a mutation of the LOS rate happens at the recognition moment, that is to say, when a flare does not work, a step-jump of the LOS rate or the overload will happen, as Figure 3(b) depicts. As explained in [27], the step jump of the LOS rate has a significant impact on the guidance command for the limitation of the guidance system, which also agrees with the opinion in [32].

According to above description, two main phases for the LOS rate are included. One is from the flare coming into the field of view (FOV) at the recognition moment, and the other starts from the recognition moment to the time that the missile body recovers to the stable tracking state. The former compels the optical axis directing to the energy central leading the LOS rate to change slightly to the wrong direction, while the latter requires the optical axis to rapidly direct to the target and then gradually recover to the stable tracking state. To lower the effects of the step-jump behavior, we first establish the following engagement model by the inspiration of [32] where it is often assumed that the horizontal and vertical planes can be decoupling controlled for the missile [15]. Moreover, the IR seeker is assumed to direct to the radiation source during the flight. Once the recognition algorithm is unable to identify the target, the seeker will track the energy central within the FOV, while if the target is identified, the orientation of the optical axis rapidly shifts from the energy central to the "right" direction, which leads to a step-jump problem for the LOS rate and overload.

Figure 4 illustrates the schematic diagram of this process, where C denotes the energy central; y_{jump} represents the step-jump amplitude of the trace point (after recognition); λ is the LOS angle before the step-jump happens; $\Delta\lambda_{\text{jump}}$ is the variation range of the LOS; h_c and h_m are the heights of the energy central and the missile, respectively; n_t and n_m are the overloads of the target and the missile perpendicular to the sight, respectively; R_{tm} is the distance between the missile and the target; and R_{cm} represents the distance between the missile and the trace point. v_t and v_m represent the speed of the target and the missile, respectively.

Motivated by the analytical method of [32], the LOS angle λ can be expressed as

$$\lambda = \arcsin\left(\frac{y}{R_{cm}}\right), \tag{1}$$

where $y = h_c - h_m$, $R_{cm} = v_c \times t_{go}$, and $t_{go} = t_f - t$. t and t_f represent the current time and the total flight time of the engagement, respectively. v_c is the relative speed between the missile and the trace point.

The initial direction of the LOS is assumed to be parallel to the x-axis in the inertial coordinate system. Since the LOS rate $\dot{\lambda}$ is small and approximately equal to zero, the amplitude of the LOS angle λ is little. Thus, in the range of $\lambda < 14^\circ$, $\sin(\lambda)$ can be approximated as λ, which is attributed to the head-on or tail-on scene.

According to the small-angle approximation, Equation (1) can be rewritten as

$$\lambda = \frac{y}{R_{cm}} = \frac{y}{v_c t_{go}}. \tag{2}$$

Let $t(0)$ be the moment when the seeker recognizes the target, then the state equation of the proportional navigation (PN) model with the overload limitation can be described as

$$\begin{cases} \dot{x}_1 = x_2, & x_1(0) = y_{\text{jump}}, \\ \dot{x}_2 = n_t - \rho_n \text{sat}\left(\dfrac{N v_c \dot{\lambda}}{\rho_n}\right), & x_2(0) = 0, \end{cases} \tag{3}$$

where x_1 and x_2 are the relative distance and speed, which are perpendicular to the LOS, respectively; N denotes the ratio

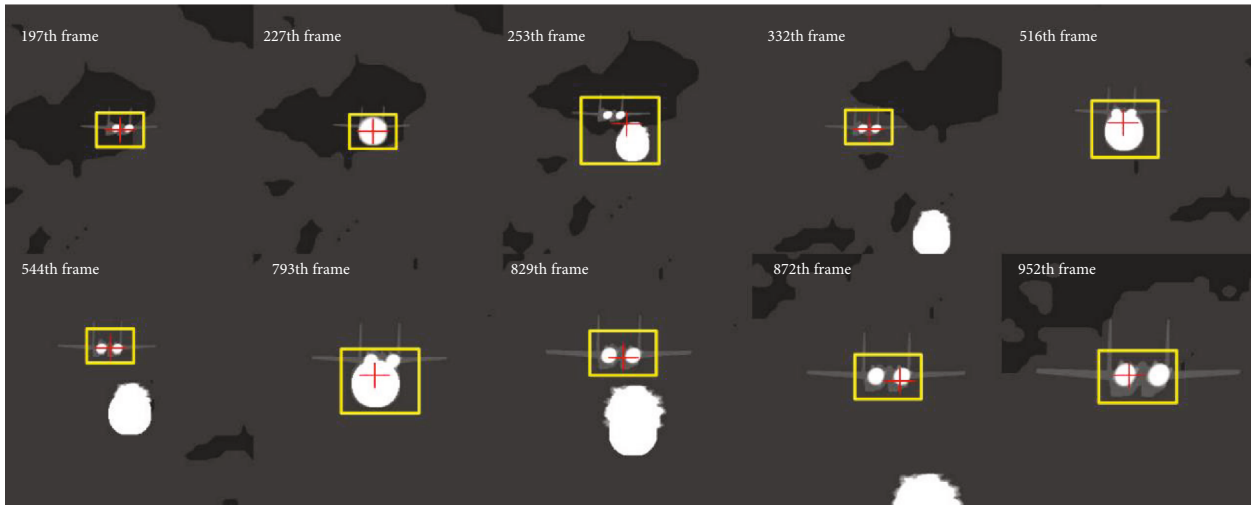

Figure 2: Simulated IR image sequences in the field of view.

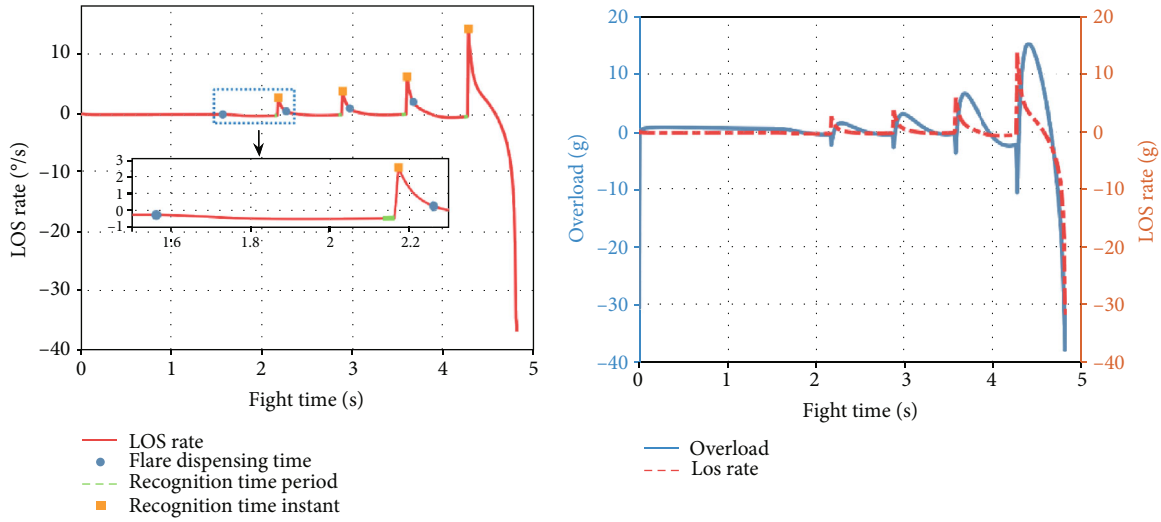

Figure 3: The variation of the LOS rate and overload. (a) The variation of the LOS rate in different time periods. (b) The variation of the overload with respect to the LOS rate.

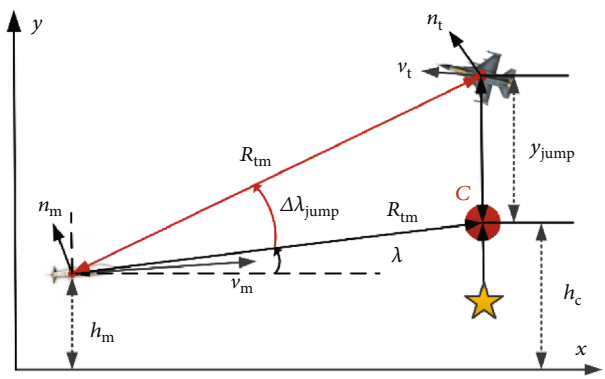

Figure 4: Schematic diagram of the step-jump phenomenon of the trace point.

coefficient and $N \geq 2$; and ρ_n represents the upper limit of the overload. The saturation function sat() is given by

$$\text{sat}(x) = \begin{cases} x, & |x| \leq 1, \\ 1, & x > 1, \\ -1, & x < -1. \end{cases} \tag{4}$$

Differentiating Equation (2) with respect to t yields

$$\dot{\lambda} = \frac{x_1 + t_{go} x_2}{v_c t_{go}^2}. \tag{5}$$

For analyzing the effects of the flare countermeasures, here, we assumed the target takes no maneuver, namely, $n_t = 0$, which is in close agreement with other studies

[27, 33, 34]. Then, substituting Equation (5) into Equation (3) yields

$$\begin{cases} \dot{x}_1 = x_2, & x_1(0) = y_{jump}, \\ \dot{x}_2 - \rho_n \mathrm{sat}\left(\dfrac{N}{\rho_n t_{go}^2}\left[x_1 + t_{go}x_2\right]\right), & x_2(0) = 0. \end{cases} \tag{6}$$

As shown above, Equation (6) represents the terminal guidance model under the step-jump circumstance, which is similar to the equation in [32]. However, Gutman only stated a standard PN block diagram and did not consider the effects of the countermeasure in [32]. Hence, as the difference of the initial state, the final equation is a little bit different. Based on this model, we will analyze the step-jump problem from the views of LOS rate and miss distance in the next section.

3. Effect Analysis of the Step-Jump Behavior

3.1. Influence of Step-Jump Behavior on the LOS Rate. In Equation (6), x_1 denotes the quadratic integral of the relative acceleration. If the relative acceleration is in saturation for a long time, which means the velocity of the missile is not enough to chase the target, namely, the relative distance x_1 will diverge and even miss the target. It can be seen from [22] that, during the engagement, the LOS rate changes the most when the step-jump behavior occurs. On the other hand, an approximately linear relationship holds between the LOS rate and overload within the PN framework. Therefore, it only needs to prevent the overload reaching the saturation state at the initial moment as suggested in [32].

$$\frac{N y_{jump}}{t_f^2} \le \rho_n, \tag{7}$$

or

$$y_{jump} \le \frac{\rho_n t_f^2}{N}. \tag{8}$$

Since $\dot{\lambda}_0 = y_{jump}/v_c t_f^2$, substituting Equation (8) in it, then we have

$$\left|\dot{\lambda}_0\right| \le \frac{\rho_n}{N v_c}. \tag{9}$$

Now, introducing a first-order delay system as

$$G_M(s) = \frac{1}{\tau s + 1}. \tag{10}$$

where τ is the time constant of the guidance system. At this point, Equation (6) can be rewritten as

$$\begin{cases} \dot{x}_1 = x_2, & x_1(0) = y_{jump}, \\ \dot{x}_2 = -n_l, & x_2(0) = 0, \\ \dot{n}_l = \dfrac{\rho_n \mathrm{sat}\left(N v_c \dot{\lambda}/\rho_n\right) - n_l}{\tau}, & n_l(0) = 0. \end{cases} \tag{11}$$

The system block diagram corresponding to Equation (11) is shown in Figure 5 [32].

In order to obtain the limit value of the LOS rate, we assume that the overload at the initial moment is equal to the maximum or minimum value, namely, $n_c = \pm\rho_n$. Let $x_1(t_f) = 0$ for a possible small miss distance, then substituting them into Equation (11), then we can obtain

$$\left|y_{jump}\right| = \tau^2 \rho_n \left(1 - e^{-\zeta}\right) + \frac{1}{2}\rho_n t_f^2 - \tau t_f \rho_n, \tag{12}$$

where $\zeta = t_f/\tau$ is defined as the standardized flight time.

In the meantime, according to Equation (9), the maximum LOS rate $\dot{\lambda}_{ideal}$ is described by

$$\dot{\lambda}_{ideal} = \frac{\rho_n}{2 v_c}. \tag{13}$$

Integrating Equation (9), we utilized the normalized initial LOS rate, which was defined in [32], to reflect the variation of the LOS rate in the step-jump moment

$$\frac{\left|\dot{\lambda}_0\right|}{\dot{\lambda}_{\mathrm{ideal}}} < \left\{1 - \frac{2}{\zeta}\left[1 - \frac{1 - e^{-\zeta}}{\zeta}\right]\right\}. \tag{14}$$

In contrast with [32], we find the results are the same, which implies that the upper bound of the normalized initial LOS rate is only associated with the time constant of the guidance system and total flight time when no first-order function exists. The results caused by the relative distance deviation or the relative velocity deviation are the same. It is worth remarking that $\dot{\lambda}_0$ in [32] means the moment that the overload reaches the saturation, while in our manuscript, it is the time when the step-jump behavior happens.

Meanwhile, the variation of the normalized LOS rate is shown in Figure 6.

As shown in Figure 6, the upper bound of $|\dot{\lambda}_0|$ increases with the increase of the standardized flight time and then gradually tends to a constant. Hence, it should be noted that there are two possible ways to increase the standardized flight time: one is to increase t_f, namely, extending the launch distance of the missile; the other is to reduce τ, i.e., accelerating the system response. Once the launch distance is extended, the smaller the LOS rate achieves with the identical step-jump behavior, then the easier the seeker can meet the requirement. When the time constant gets shorter, the response of the seeker turns faster, and then the LOS rate can reach its maximum value rapidly.

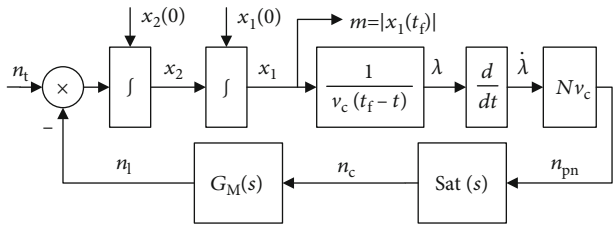

Figure 5: Block diagram of the numeric derivative terminal guidance system.

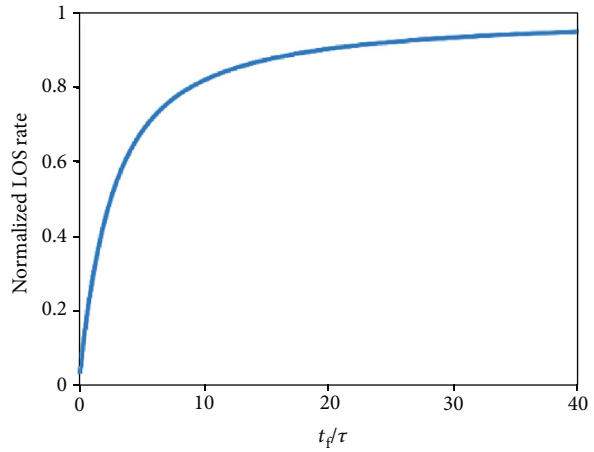

Figure 6: The upper bound of the normalized LOS rate in two-dimensional space.

Meanwhile, if the first-order system is a nonminimum phase system as follows

$$G_M(s) = \frac{1 + d\tau s}{1 + \tau s}, \tag{15}$$

where d is the delay coefficient with the constraints $|d| \leq 1$. When $d > 0$, it means Equation (15) is a minimum phase delay system, while if $d < 0$, it means $G_M(s)$ is a nonminimum phase delay system. Thus, the system state given by Equation (11) can be rewritten as

$$\begin{cases} \dot{x}_1 = x_2, & x_1(0) = y_{\text{jump}}, \\ \dot{x}_2 = -x_3 - dn_c, & x_2(0) = 0, \\ \dot{x}_3 = \dfrac{-x_3 + (1-d)n_c}{\tau}, & x_3(0) = 0. \end{cases} \tag{16}$$

Let $x_1(t_f) = 0$, then Equation (16) can be solved as

$$\frac{\left|\dot{\lambda}_0\right|}{\dot{\lambda}_{ideal}} < \left\{1 - \frac{2}{\zeta}(1-d)\left[1 - \frac{1-e^{-\zeta}}{\zeta}\right]\right\}. \tag{17}$$

Comparing the results with [32], it suggests that the upper bound of the normalized initial LOS rate is actually affected by the delay coefficient except the aforementioned two coefficients.

The corresponding variation trends are shown as follows.

As shown in Figure 7(a), the upper bound of the normalized LOS rate increases from the negative value when $d < 0$, which costs the missile body more time to turn around. Hence, the longer the turning time is, the closer the target is, or the less the adjustment time is, then the more difficult the strike is, while, when $0 < d < 1$, $|\dot{\lambda}_0|$ is obviously greater, which makes the missile turn around more quickly and complete the strike. Meanwhile, as seen from Figures 7(b)–7(e), $|\dot{\lambda}_0|/\dot{\lambda}_{\text{ideal}}$ is most affected by parameter d, followed by parameter τ, and finally parameter t_f, and the less the time constant is, or the larger the flight time is, or the closer the delay coefficient is to 1, then the closer the normalized LOS rate approaches to 1, which can allow the missile to reflect more quickly.

In conclusion, the underlying reason for the large miss distance is the LOS rate cannot, as soon as possible, reach the ideal value due to the system delay when the trace point jumps. Meanwhile, the upper bound of the normalized LOS rate is related to the first-order system and the standardized flight time. Here, the closer the delay coefficient d is to 1, or the larger the standardized flight time ζ is, and the faster the missile responds, the greater the LOS rate changes, then the easier it is for the missile to track and strike the target. At the same time, since the upper bound of the normalized LOS rate is gradually stabilized when arriving at a certain value, the adjustment of τ is not necessary to have an infinite reduction.

3.2. Influence of Step-Jump Behavior on the Guidance Precision. To further analyze the impacts of the step-jump behavior on the guidance precision, the adjoint method is introduced [27]. It is worth noting that the LOS can be obtained by solving Equation (2) where the relative velocity is adopted directly. However, the variation in the velocity cannot be accurately obtained by the current engagement. Accordingly, Equation (6) belongs to the analytical differential model, and the corresponding system block diagram with PN framework is illustrated in Figure 8.

To derive an adjoint system from the block diagram in Figure 8, the following three steps are required:

(1) Convert all the system inputs to impulses. In order to construct an adjoint, we must have impulsive inputs in the original system. Since impulsive inputs may not exist in the original system, block diagram manipulation of the actual inputs of the original system may be necessary. In our cases, deterministic input, such as n_t, can be converted to impulsive inputs by judicious use of integrators. Meanwhile, the initial condition, like $x_1(0)$ and $x_2(0)$, are equivalent at the integrator output to an integrator with an impulsive input

(2) Replace the time-varying coefficient t in the original system to $t_f - t$ and convert the $t_f - t$ in the original system into t

(3) Reverse the direction of the signal flow in the original system and redefine nodes as summing junctions and vice versa

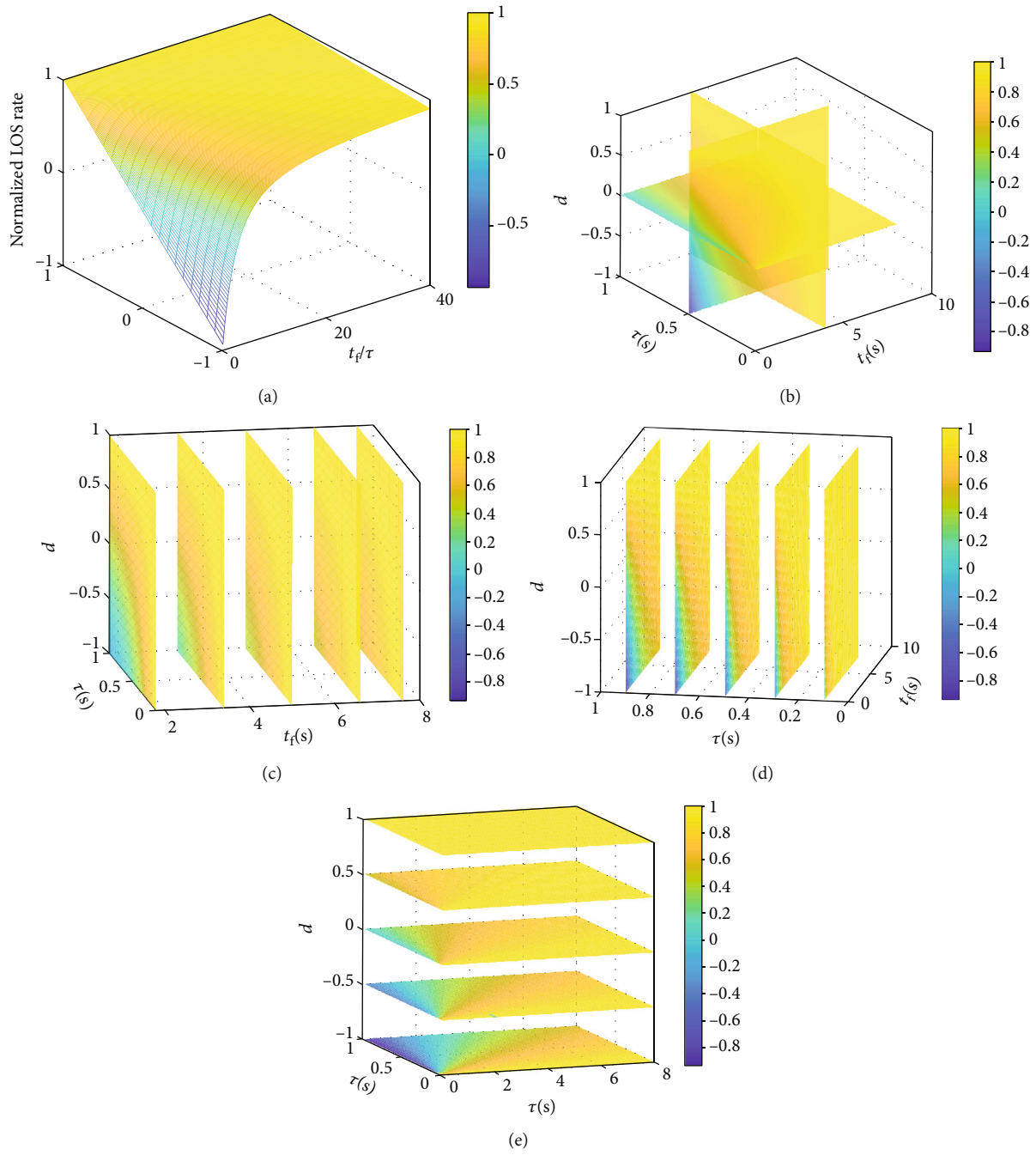

FIGURE 7: Variation of $|\dot{\lambda}_0|/\dot{\lambda}_{ideal}$ with respect to t_f and d in three-dimensional space. (a) The upper bound of the normalized LOS rate in three-dimensional space. (b) Variation of $|\dot{\lambda}_0|/\dot{\lambda}_{ideal}$ with respect to t_f, τ, and d. (c) Variation of $|\dot{\lambda}_0|/\dot{\lambda}_{ideal}$ with respect to τ and d. (d) Variation of $|\dot{\lambda}_0|/\dot{\lambda}_{ideal}$ with respect to t_f and d. (e) Variation of $|\dot{\lambda}_0|/\dot{\lambda}_{ideal}$ with respect to t_f and τ.

Following the above steps, the linear systems depicted in Figures 5 and 8 are equivalent to the adjoint systems illustrated in Figures 9 and 10.

In Figure 9, x_1-x_3 represent the corresponding pulse inputs of the original system, respectively. Here, x_1 represents the sensitivity of the trace point position error to the miss distance, and $x_1 = \delta(t)$, where $\delta(t)$ means a pulse function. Besides, this equation indicates that a step-jump behavior occurs at the initial time. x_2 represents the sensitivity of the heading error to the miss distance, which is equal to 0. x_3 denotes the sensitivity of the LOS angle error to the miss distance, which is also 0. The output MTD (Miss Distance due to Target Displacement) indicates the miss distance caused by the variation of the trace point position, and DIC (Initial Condition of Dish Angle) means the miss distance arising from the deviation of the LOS angle. It can be seen from Figure 9 that the error of the trace position has been indirectly fed back to the heading error, and the total miss

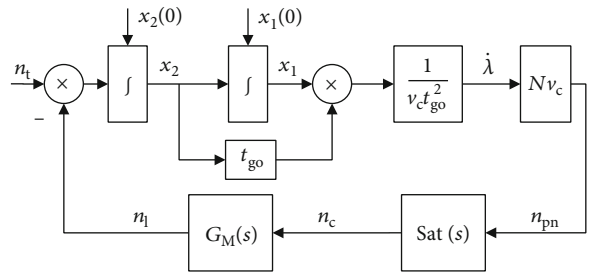

Figure 8: Block diagram of the analytic terminal guidance system.

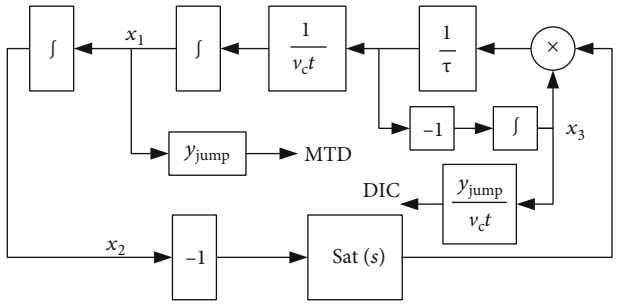

Figure 9: Adjoint block diagram of the numeric derivative model.

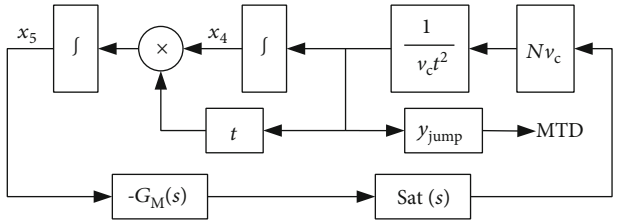

Figure 10: Block diagram of the analytic derivative adjoint model.

distance is therefore equal to the sum of the miss distance MTD, which is caused by the trace position error, and the miss distance DIC, which is caused by the LOS angle error.

Figure 10 illustrates the block diagram of the analytic derivative adjoint model.

Parameters x_4 and x_5 in Figure 10 indicate the effect of x_1 and x_2 given in Figure 9, and here, $x_4 = \delta(t)$ and $x_5 = 0$. In this analytical differential model, since the resolved LOS rate is the true LOS rate of the missile, no miss distance is increased for the deviation of the LOS angle. Accordingly, the miss distance can be described by MTD.

To validate the effectiveness of the aforementioned adjoint systems, the results are compared to the miss distance obtained under the nonlinear system. First of all, we will briefly introduce the nonlinear system where λ_t is given by

$$\lambda_t = \arctan\left(\frac{y_t}{x_t}\right). \tag{18}$$

Differentiating Equation (18) with respect to t yields

$$\dot{\lambda}_t = \frac{d}{dt}\left(\arctan\left(\frac{y_t}{x_t}\right)\right) = \frac{x_t\dot{y}_t - \dot{x}_t y_t}{R_t^2}. \tag{19}$$

Then, we introduce a time delay system in the seeker system

$$\ddot{\lambda}_t^c = \frac{\dot{\lambda}_t - \dot{\lambda}_t^c}{\tau}, \tag{20}$$

where $\dot{\lambda}_t^c$ is the actual output of the LOS rate and $\ddot{\lambda}_t^c$ means the second-order derivative of the LOS angle.

By taking the time delay and limitation of the overload into account, the actual output overload can be expressed as

$$n_c = \rho_n \mathrm{sat}\left(\frac{Nv_c\dot{\lambda}_t^c}{\rho_n}\right). \tag{21}$$

To this end, the main procedures are given, and more details can be found in [27].

3.3. Validity Verification of the Adjoint System. The simulation is performed to compare with the nonlinear model to validate the effectiveness of the two adjoint models in analyzing the guidance precision. Here, we set the head-on situation as an example, and the initial parameters used in simulations are given in Table 1, where the gravitational acceleration $g = 9.8\,\mathrm{m/s^2}$ and the sampling period $T_s = 0.01\,\mathrm{s}$.

With the above settings, the miss distance for the three systems are illustrated in Figure 11.

Figure 11 shows the miss distances of each system for different flight times. As shown above, the miss distance curves of the adjoint models coincide with each other, indicating that their performance is comparable. At the same time, the difference between the miss distance of the adjoint model and the nonlinear model is more than 10 m in the initial phase, and the error between them is gradually increasing. This is mainly because the construction of the adjoint system is based on a linear model, which is less sensitive to the time delay than the nonlinear model. However, the adjustment of the nonlinear model is slower for the effects of the time delay, which makes a gap with the above adjoint models. Once the nonlinear model is fully responsive, then the downward trend of the miss distance is almost the same with the adjoint models. The most important is that the miss distance of the adjoint model is consistent with the miss distance of the nonlinear system, which indicates that the established adjoint models are effective.

To further figure out the consistency of the miss distance derived from the adjoint models, an experiment is conducted, and the results are shown in Figure 12.

Figure 12 shows how MTD and DIC change in the numerical derivative adjoint system. Seen in this perspective, DIC continues to increase while MTD decreases during the initial period, while since the augment rate of DIC is weaker than the decrement rate, the descending rate of the miss distance appears obviously greater than the later period. After a period of response stage for the system, the LOS angle has been adjusted and completely points to the target, then the miss distance keeps almost stable. Overall, the analysis above reveals that the performance of the established adjoint systems is comparable and, at the same time, is close enough

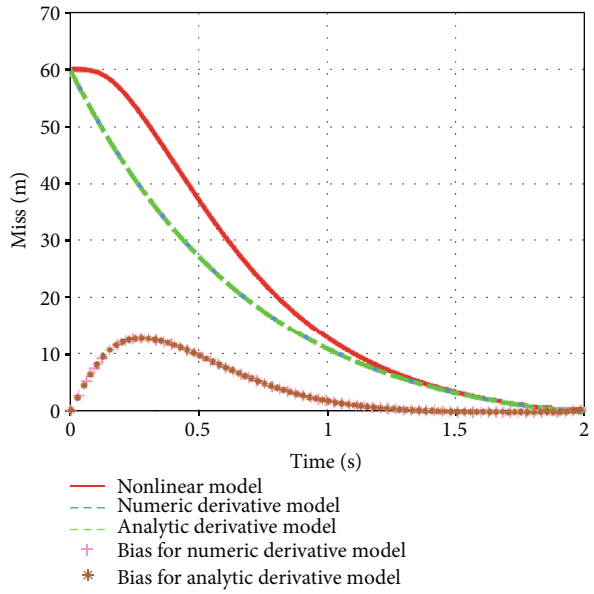

Figure 11: Comparison of the miss distance index between three systems.

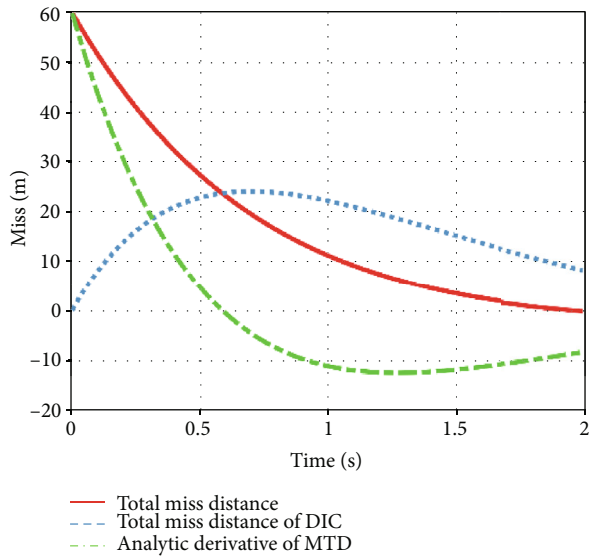

Figure 12: The change of miss distance of the numeric derivative adjoint model.

to that of the nonlinear system. Thus, the effects of the influencing factors to the final results are to be checked by the simulation with the adjoint systems, through which we can acquire the main influencing factors and design a more targeted anti-step-jump guidance.

3.4. Analysis of the Influencing Factors. Following the above analysis, we then apply the adjoint system shown in Figure 9 to analyze the impact of the ratio coefficient, time constant, and amplitude of the step-jump on the miss distance when the step-jump behavior happens at the initial moment. Moreover, the other related parameters can be seen in Table 2, and the variation curve of the miss distance with respect to the ratio coefficient is shown in the following.

Figure 13 suggests that the miss distance generally converges with the increase of the flight time, which illustrates that the miss distance is in reverse ratio to the relative distance when the step-jump phenomenon happens. Meanwhile, it should be noted that the miss distance falls faster with the ratio coefficient increasing in the early stage. But in the end, the larger the ratio coefficient is, the worse it gets in the view of the miss distance. So we learn that a large ratio coefficient has stronger adjustment capability once the step-jump behavior happens, but it is also readily available with excessive adjustment and leads to a large miss distance in the end. Therefore, we can learn from this analysis that the missile can adopt a variable ratio coefficient strategy to achieve the optimal guidance accuracy within the limit to the flight time.

The variation of the miss distance with the time constant is shown in Figure 14.

As shown in Figure 14, the time constant has a great impact on the terminal accuracy. The smaller the time constant is, the faster the guidance system will eliminate the deviation caused by the jump of the trace point. However, the time constant of the missile is determined during manufacture. Therefore, using higher agility devices will greatly improve the anticountermeasure ability of the missile.

Next, we proceed to study the influences of the jump amplitude of the trace point.

Figure 15 shows the influence of the jump amplitude on the miss distance. Meanwhile, to some extent, the jump amplitude of the trace point reflects the recognition efficiency of the IR seeker system. The jump amplitude performs a direct relationship to the required overload, and the stronger the trace point jumps, the higher the overload the missile requires. Moreover, the recovery time for the missile body gets longer. Once the remaining time is insufficient, the strike must be a failure. Basically, the seeker needs to identify the target as quickly as possible to decrease the jump amplitude, which can greatly improve the guidance accuracy of the missile. Shortening the recognition time will not only make the jump amplitude smaller but also save the remaining time, providing the possibility for the subsequent adjustment of the missile.

In the end, it can be concluded that the ratio coefficient, the time constant, and the jump amplitude of the trace point have a great influence on the terminal accuracy. If the time constant is fixed, the larger ratio coefficient is beneficial for the missile to accelerate the convergence of the miss distance within the change scope of the overload. Similarly, the higher efficiency of the recognition process is useful to improve the terminal accuracy.

4. Simulation Results

Based on the above analysis, within the PN framework, the LOS rate and overload command at the moment the step-jump behavior approaches a large value, even infinity, when there is very little remaining flight time left, which can be seen in Figure 3. Thus, to address this challenge, we introduce a saturation function to limit the acceleration command. The saturation value can be fixed at a value which equals half of

the maximum acceleration capability of the missile, and the length of the saturation is set to be three or five sampling periods. Hence, the anti-step-jump guidance (ASJG) can be described by

$$n_c^{ASJG} = \begin{cases} Nv_c\dot{\lambda}_t^c, & \text{others}, \\ \dfrac{\rho_n}{v}\,\mathrm{sat}\left(\dfrac{Nv_c\dot{\lambda}_t^c}{\rho_n}\right), & t \in \left[t_0', t_0' + \pi \cdot T_s\right] \cup \left[t_1', t_1' + \pi \cdot T_s\right] \cup \cdots \left[t_\kappa', t_\kappa' + \pi \cdot T_s\right], \end{cases} \tag{22}$$

where v means the limitation scale of the overload (here, we have $v = 5/7$); κ represents the number of jumps; π is the length of the saturation for each step-jump behavior, and $\pi = 5T_s$; T_s denotes the sampling period for the guidance system; and t_κ^j means the initial moment of the κ-th step-jump behavior.

Meanwhile, the compared guidance laws selected in this study are proportional navigation guidance (PNG), adaptive slide mode guidance (ASMG) [35], and optimal guidance (OG) [36]. The corresponding expressions are shown as follows.

PNG can be given by

$$n_c^{PNG} = n_c^{PN} = Nv_c\dot{\lambda}_t^c. \tag{23}$$

ASMG can be expressed as

$$n_c^{ASMG} = Nv_c\dot{\lambda}_t^c + \varepsilon\frac{\dot{\lambda}_t^c}{\left|\dot{\lambda}_t^c\right| + \delta}, \tag{24}$$

where $\varepsilon = 60$ and $\delta = 0.001$.

OG can be expressed as

$$n_c^{OG} = \frac{N'}{t_{go}^2}\left[x_1 + x_2 t_{go} - n_l\tau^2(e^{-x} + x - 1)\right], \tag{25}$$

where $x = t_{go}/\tau$ and N' is the variable ratio coefficient, which can be derived by

$$N' = \frac{6x^2(e^{-x} - 1 + x)}{2x^3 + 3 + 6x - 6x^2 - 12xe^{-x} - 3e^{-2x}}. \tag{26}$$

As shown above, the implementation of PNG and ASMG only requires the seeker to provide the LOS rate, which is easy to achieve. The OG system, on the other hand, requires more accurate t_{go} information. Here, the estimation method of t_{go} in [36] is used, and the underlying simulations include head-on and tail-on situations where the trace point jumps to the target when $t_{go} = 3$ s. The time constant $\tau = 0.6$ s, the jump amplitude $y_{jump} = 150$ m, and the remaining parameters are given in Table 1.

Before we implement the experiments, some simplifying assumptions should be listed in the followings.

Assumption 1. The target takes no maneuvers in the engagement.

Assumption 2. Once the step-jump behavior happens, the guidance system can reflect at the first moment.

In fact, the maneuvering has great coupling relationship with the countermeasure factors, which has been mentioned in [37, 38]. In order to simplify the analysis, here we suppose the target takes no maneuvers for paying attention to the step-jump behavior caused by the flares, while in [38], we have tried to construct a model to describe their relationships in the view of environmental complexity quantification. Besides, we assume the step-jump behavior can be detected by the missile and then have a quick response. The related works about the step-jump timing has been investigated in [37], and with the constructed model, we also can obtain the separation timing with a high accuracy.

4.1. Test on Head-On Scenario. The trajectories of the missile and the trace point are shown in Figure 16, and the solid red and blue circles mean the initial position of the energy central and the missile, respectively.

Figure 16 illustrates the trajectories and overloads of different guidance laws. For convenience, we separate the tracking process into two phases: phase 1 means tracking the false target, namely, the energy central, and phase 2 is to track the true target after the step-jump behavior. As shown in Figure 16(a), the trajectory of ASJG is smoother than others, which means it costs less energy to strike the target. Meanwhile, the corresponding miss distances of PNG, OG, ASMG, and ASJG are 16.83 m, 3.55 m, 4.52 m, and 2.78 m, respectively. Thus, in terms of the guidance accuracy, our proposed ASJG performs the best, OG is the second, then ASMG, and PNG is the worst. Actually, we can generally acquire the reason from Figure 16(b), that is, ASJG alleviates the influence of the step-jump behavior by the effect of the continuous saturation, which can shorten the adjustment time for the overload and save the energy to strike the target. Likewise, OG can achieve a higher strike efficiency then ASMG and PNG. However, OG needs not only the prior information of the

Table 2: Initial simulation parameter setting.

	Parameter	Meaning	Value
Missile	N	Ratio coefficient	3
	v_m	x-axis velocity	400 m/s
	x_m	x and y-axis position	(0, 1000) m
	ρ_n	Upper bound of the overload	35 g
	τ	Time constant	1 s
	y_{jump}	Amplification of the step jump in y-axis direction	60 m
Target	v_t	x-axis velocity	200 m/s
	x_t	x and y-axis position	(3200, 1000) m

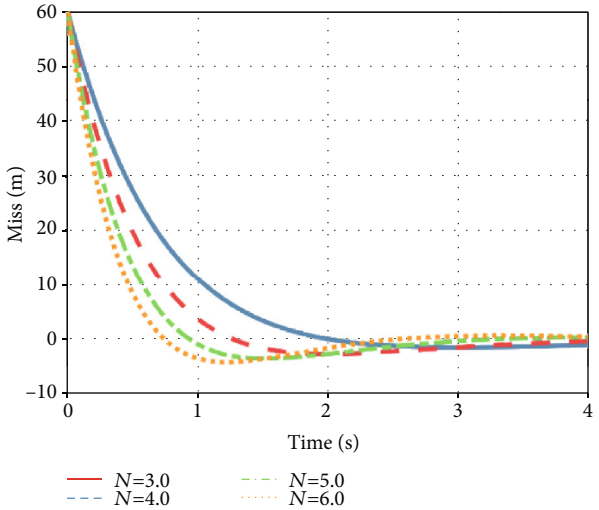

Figure 13: Influence of the ratio coefficient on the miss distance.

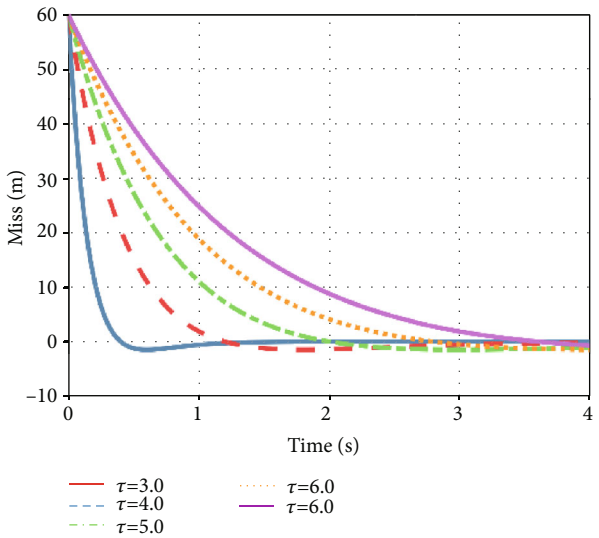

Figure 14: Influence of the time constant on the miss distance.

guidance system but also the accurate t_{go}, which is difficult to obtain. Meanwhile, ASJG needs to get the step-jump behavior, and we can use the model in [37] to estimate it for get a better performance in the step-jump scenarios.

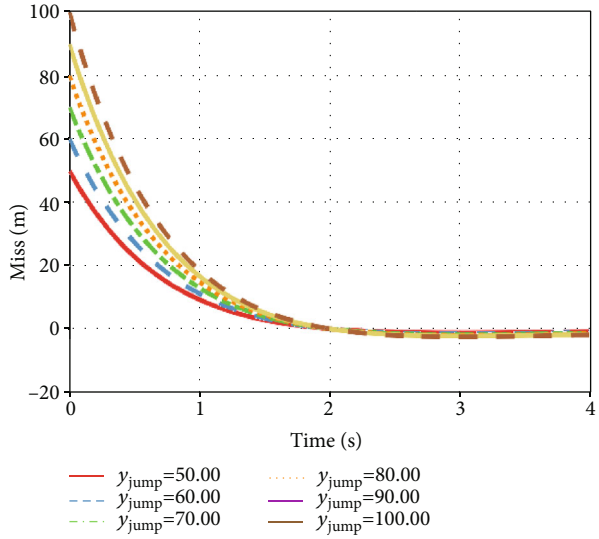

Figure 15: Influence of the jump amplitude on the miss distance.

4.2. Test on Tail-On Scenario. Here, we introduce another typical scenario to test the performance of our proposed guidance law. Figure 17 shows the results of different guidance laws.

As shown in Figure 17(a), the strike results are very close for different guidance laws, and the obtained miss distance for APG is 2.48 m, OG is 0.67 m, ASMG is 4.52 m, and ASJG is 0.72 m. Hence, our proposed ASJG can achieve a good performance as OG in the tail-on scenario. Besides, the flight times of ASJG and OG are also shorter than the other two guidances, which suggests that these two guidances are more efficient in the step-jump scenario. The variation of the overload is shown in Figure 17(b). The variation amplitude of ASJG is less than the others in phase 2. Moreover, it suggests that the standard PNG and ASMG is not suitable for the step-jump scenario for the large jump of the overload.

In summary, the following conclusions are drawn from the head-on and tail-on scenarios: the performance of the proposed ASJG is comparable to that of OG, while the performance of PNG is the worst. Furthermore, due to the long adjustment time for the overload caused by the step-jump behavior, the saturation operation in the initial stage is

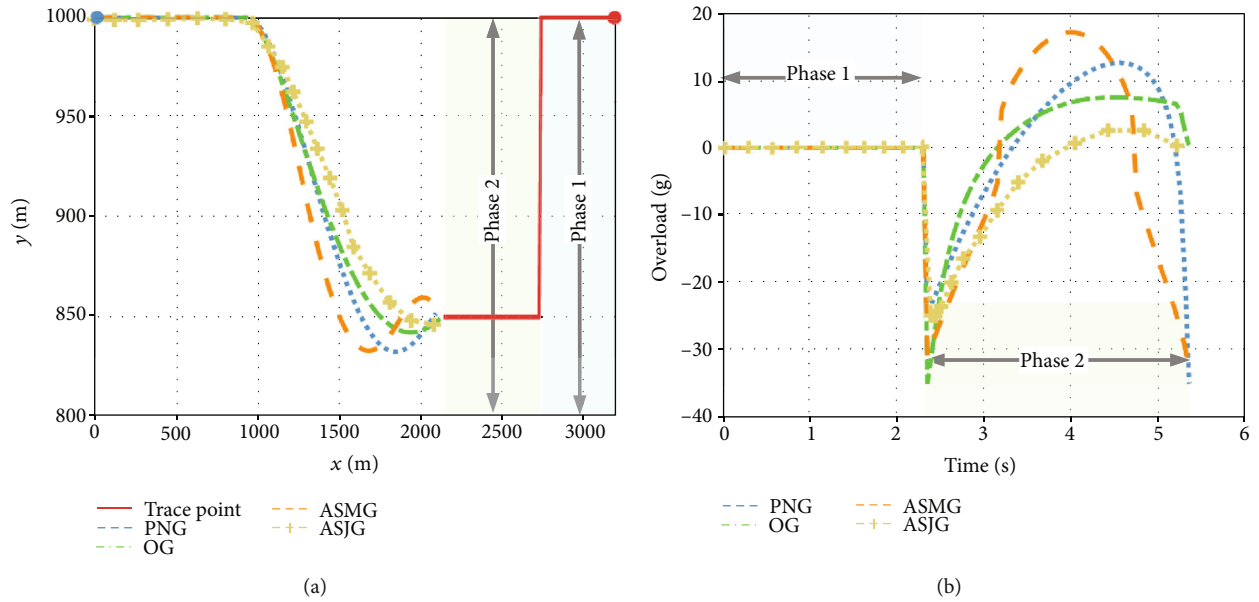

Figure 16: The variation of the state for the single-jump system in the head-on scenario. (a) Trajectories of the missile and trace point; (b) overloads of different guidance laws.

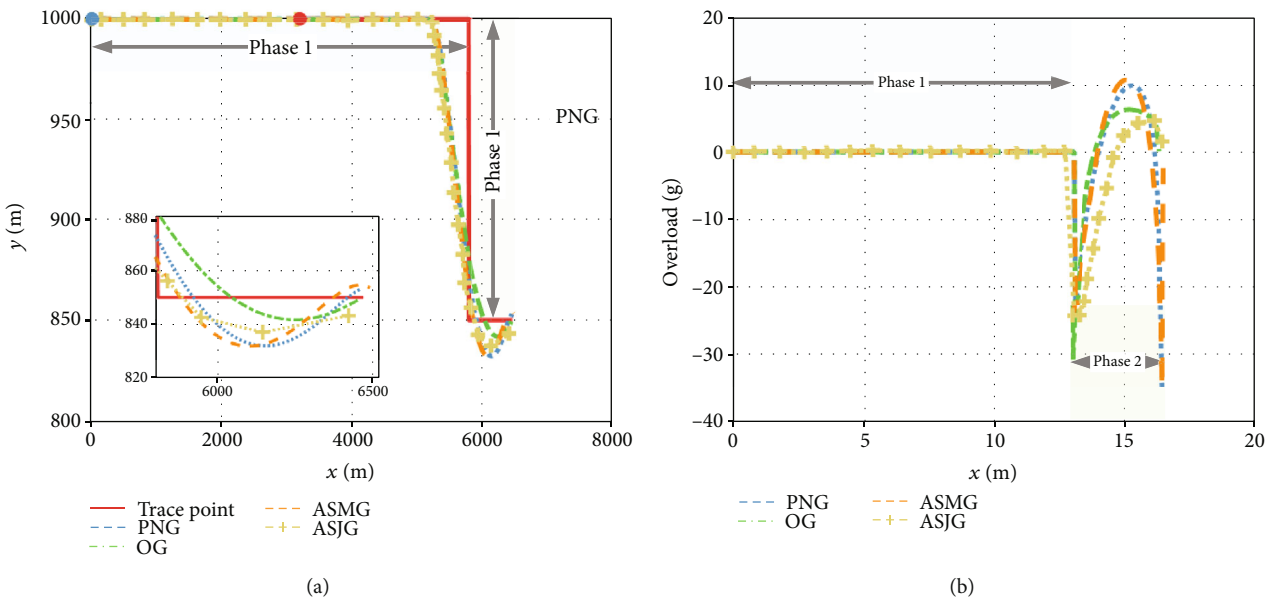

Figure 17: The variation of the state for the single-jump system in the tail-on scenario. (a) Trajectories of the missile and trace point; (b) overloads of different guidance laws.

significant to alleviate the step-jump effects and achieve a higher guidance accuracy.

5. Conclusion

Infrared flares have become the primary approach to limit IR homing missiles. To overcome the effects of the step-jump behavior caused by flares, this study not only analyzes the influence in consideration of the LOS rate and the guidance accuracy but also designs an anti-step-jump guidance law. As a result, the following conclusions are made:

(1) In the IR countermeasure circumstance, the form of the first-order system and the standardized flight time have significant impacts on the LOS rate at the step-jump moment, and the nonminimum phase system can greatly lower the guidance performance. Meanwhile, the upper bound of the normalized LOS rate increases with the standardized flight time and gradually trends to a constant, which means there is no need for unlimitedly reducing the time constant

(2) The constructed analytical differential adjoint system is effective in analyzing the miss distance in this step-

jump scenario. Besides, the ratio coefficient, time constant, jump amplitude, and recognition efficiency have significant impacts on the guidance accuracy

(3) As the released flare countermeasure takes effect, the overload will suffer a step-jump behavior and attenuate to near zero value with a long adjustment time. A saturation operation is of great utility in shortening the overload adjustment time when the step-jump behavior happens by choosing proper values in Equation (22). Meanwhile, the proposed ASJG outperforms OG, ASMG, and PNG by the constraint operation of the overload during the step-jump stage

Future work includes extending the effects of the parameters in the expression of ASJG and verifying our proposed ASJG in more realistic implementation; another effort will be spent on designing a high-efficient recognition algorithm to solve the IR flare problem fundamentally.

Data Availability

The image data used to support the findings of this study are included within the figure file. And the image data used to support the findings of this study are available from the corresponding author upon request.

Disclosure

The National Natural Science Foundation of China gave its approval to publish the current paper.

Conflicts of Interest

The authors declare that there is no conflict of interest regarding the publication of this paper.

Acknowledgments

The authors gratefully acknowledge the fund from the National Natural Science Foundation of China (approval serial number 51776200).

References

[1] S. Wu, S. Niu, K. Zhang, and J. Yan, "An aircraft tracking method in simulated infrared image sequences based on regional distribution," in *Image and Video Technology. PSIVT 2017*, Lecture Notes in Computer Science, S. Satoh, Ed., pp. 343–355, Springer, Cham, Switzerland, 2017.

[2] Y. Cao, G. Wang, D. Yan, and Z. Zhao, "Two algorithms for the detection and tracking of moving vehicle targets in aerial infrared image sequences," *Remote Sensing*, vol. 8, p. 28, 2016.

[3] A. Berg, J. Ahlberg, and M. Felsberg, "A thermal object tracking benchmark," in *2015 12th IEEE International Conference on Advanced Video and Signal Based Surveillance (AVSS)*, pp. 1–6, Karlsruhe, Germany, August 2015.

[4] K. N. Chopra, "Analysis and modeling of IR signatures by optoelectronic techniques and countermeasures - a technical tutorial and review," *Latin-American Journal of Physics Education*, vol. 12, 2018.

[5] M. Wan, G. Gu, W. Qian et al., "Total variation regularization term-based low-rank and sparse matrix representation model for infrared moving target tracking," *Remote Sensing*, vol. 10, no. 4, p. 510, 2018.

[6] J. X. Fan and J. Y. Yang, "Trends in infrared imaging detecting techonlogy," in *Electro-Optical and Infrared Systems: Technology and Applications X*, vol. 8896, Dresden, Germany, 2013.

[7] M. D. Withey, "Infrared countermeasure flares," *The Imaging Science Journal*, vol. 58, no. 5, pp. 295–299, 2013.

[8] E. C. Koch, "2006-2008 annual review on aerial infrared decoy flares," *Propellants, Explosives, Pyrotechnics*, vol. 34, no. 1, pp. 6–12, 2009.

[9] T. W. Bae, B. L. Kim, Y. C. Kim, and S. H. Ahn, "Jamming effect analysis of infrared reticle seeker for directed infrared countermeasures," *Infrared Physics & Technology*, vol. 55, no. 5, pp. 431–441, 2012.

[10] D. Perh, *A study into advanced guidance laws using computational methods*, Monterey, California, Naval Postgraduated School, 2011.

[11] L. Dawei, Q.-l. Xia, Y.-l. Du, and T.-t. Zuo, "Miss distance and impact angle error of trajectory shaping guidance law based on statistical linearization adjoint method," *Energy Procedia*, vol. 13, pp. 6370–6377, 2011.

[12] X. du, R. Lv, H. Tu, and C. Jiang, "The research on infrared seeker with disturbance rejection effect parasitic," *Optik*, vol. 170, pp. 409–419, 2018.

[13] C.-L. Lin and Y.-Y. Chen, "Design of fuzzy logic guidance law against high-speed target," *Journal of Guidance, Control, and Dynamics*, vol. 23, no. 1, pp. 17–25, 2000.

[14] L. Shiyong and Z. Qian, *Intelligent Guidance–Intelligent Adaptive Guidance Laws for Homing Missile*, Harbin Institute of Technology Press, Harbin, 2011.

[15] Y.-L. Lee, K.-Y. Chen, and S.-J. Liao, "Using proportional navigation and a particle swarm optimization algorithm to design a dual mode guidance," *Computers and Electrical Engineering*, vol. 54, pp. 137–146, 2016.

[16] P.-f. Yang, Y.-w. Fang, Y.-l. Wu, and X.-j. Yong, "Finite-time convergent terminal guidance law design based on stochastic fast smooth second-order sliding mode," *International Journal for Light and Electron Optics*, vol. 127, no. 15, pp. 6036–6049, 2016.

[17] Y. Xu, Y. Fang, W. Peng, and Y. Wu, "An efficient Gaussian sum filter based on prune-cluster-merge scheme," *IEEE Access*, vol. 7, pp. 150992–151005, 2019.

[18] Z. Liu, S. Chen, H. Wu, and K. Chen, "Robust Student's t mixture probability hypothesis density filter for multi-target tracking with heavy-tailed noises," *IEEE Access*, vol. 6, pp. 39208–39219, 2018.

[19] Z. H. Li, L. Ning, and S. N. Xu, "Nonlinear non-Gaussian system filtering based on Gaussian sum and divided difference filter," *Control and Decision*, vol. 27, no. 1, pp. 129–134, 2012.

[20] Q. Lin, J. J. Yin, J. Q. Zhang, and B. Hu, "Gaussian sum filter methods for nonlinear non-Gaussian models," *Systems Engineering and Electronics*, vol. 32, no. 12, pp. 2493–2499, 2010.

[21] M. Polasek, J. Nemecek, and I. Q. Pham, "Counter countermeasure method for missile's imaging infrared seeker," in *2016 IEEE/AIAA 35th Digital Avionics Systems Conference (DASC)*, pp. 25–29, Sacramento, CA, USA, 2016.

[22] D. Yang, Y. X. Cao, J. Li, F. F. Xue, and M. M. Song, "The study on separation characteristic of airborne infrared decoy and simulation," *Infrared Technology*, vol. 40, pp. 585–589, 2018.

[23] S. Li, K. Zhang, J. Yin, and K. Yang, "A study on IR target recognition approach in aerial jamming environment based on Bayesian probabilistic model," *IEEE Access*, vol. 7, pp. 50300–50316, 2019.

[24] S. Wu, K. Zhang, S. Niu, and J. Yan, "Anti-interference aircraft-tracking method in infrared imagery," *Sensors*, vol. 19, no. 6, p. 1289, 2019.

[25] J. R. White, "Aircraft infrared principles, signatures, threats, and countermeasures," Technical Report; Naval Air 410 Warfare Center Weapons div China Lake, Fort Belvoir, VA, USA, 2012.

[26] G. Y. Wang, G. Liu, N. N. Yu, and X. X. Liu, "An intelligent algorithm for infrared target recognition," in *2016 IEEE International Conference on Information and Automation (ICIA)*, Ningbo, China, August 2016.

[27] P. Zarchan, *Tactical and Strategic Missile Guidance*, American Institute of Aeronautics and Astronautics Inc Press, Reston, Virginia, 6th edition, 2012.

[28] X. Wang, *Study on performance analysis and evaluation of terminal guidance system, [Ph.D. thesis/M.S. thesis]*, Harbin Institute of Technology, 2016.

[29] A. Vermeulen and G. Maes, "Missile avoidance maneuvres with simultaneous decoy deployment," in *AIAA Guidance, Navigation, and Control Conference*, pp. 2009–6277, Chicago, Illinois, 2009.

[30] O. Goldan and S. Gutman, "Adjoint stability and miss distance in proportional navigation," *Journal of Guidance, Control, and Dynamics*, vol. 35, no. 4, pp. 1089–1093, 2012.

[31] G. J. Gray, N. Aouf, M. Richardson, B. Butters, and R. Walmsley, "Countermeasure effectiveness against an intelligent imaging infrared anti-ship missile," *Optical Engineering*, vol. 52, no. 2, article 026401, 2013.

[32] S. Gutman and O. Gutman, "Validity of linearization in guidance systems," *Journal of Guidance, Control, and Dynamics*, vol. 39, no. 8, pp. 1893–1896, 2016.

[33] O. Gutman and Z. J. Palmor, "Proportional navigation against multiple targets," *Guidance Control, and Dynamics*, vol. 34, no. 6, pp. 1728–1733, 2011.

[34] Y. F. Hu and B. F. Song, "Evaluation the effectiveness of the infrared flare with a tactic of dispensing in burst," in *2010 3rd International Symposium on Systems and Control in Aeronautics and Astronautics*, pp. 131–136, Harbin, China, 2010.

[35] D. Zhou, *New Guidance Laws for Homing Missiles*, National Defense Industry Press, Beijing, 2002.

[36] J. Z. Ben-Asher and I. Yaesh, "Optimal guidance with reduced sensitivity to time-to-go estimation errors," *Journal of Guidance, Control, and Dynamics*, vol. 20, no. 1, pp. 158–163, 1997.

[37] X. Yang, F. Yangwang, W. Youli, X. Bingsong, Z. Danxu, and L. Huan, "LOS-rate jump characteristic modelling under IR flare countermeasure circumstance," *Infrared and Laser Engineering*, vol. 48, no. 5, article 504001, 2019.

[38] N. Deqing, W. Youli, X. Yang, and X. Rui, "Quantification modeling for environmental complexity under point source infrared decoy interference," *Infrared and Laser Engineering*, vol. 49, no. 2, article 0204003, 2020.